

# HIGH RESOLUTION IMAGING X-RAY SPECTROSCOPY OF MARS

K. Dennerl <sup>a</sup>

<sup>a</sup> Max-Planck-Institut für extraterrestrische Physik, Giessenbachstraße, 85748 Garching, Germany

The first observation of Mars with *XMM-Newton*, in November 2003, has provided a wealth of novel information about the X-ray properties of our neighbouring planet. High resolution imaging spectroscopy with *RGS* clearly shows that its X-ray emission is composed of two different components: fluorescent scattering of solar X-rays on neutral molecules in its upper atmosphere, and emission from highly charged ions in its exosphere. The flux ratio in the O<sup>6+</sup> multiplet proves that these ions are of solar wind origin, interacting with the exospheric neutrals by charge exchange. This is the first definite detection of charge exchange induced X-ray emission from the exosphere of another planet. X-ray images of the Martian exosphere in individual emission lines exhibit a highly anisotropic morphology. Most of the emission is observed several 1000 km above the Martian poles. The detailed morphology, however, is different between individual ions and ionization states. With its capability to trace the X-ray emission out to at least 8 Mars radii, *XMM-Newton* proceeds into exospheric regions far beyond those that have been observationally explored to date.

## 1. Introduction

Since July 2001 we know that Mars is an X-ray source. Mars is the fourth planet which was found to emit X-rays, after the Earth [e.g. 1; 2], Jupiter [3] and Venus [4]. X-rays from Mars were first detected in 2001 with *Chandra* [5]. The morphology and the X-ray luminosity of  $\sim 4$  MW were found to be consistent with fluorescent scattering of solar X-rays in the upper Martian atmosphere. The X-ray spectrum obtained with *Chandra* ACIS-I was dominated by a single narrow emission line at 0.65 keV, which was identified as the O-K $_{\alpha}$  fluorescence line, shifted by  $\sim 120$  eV to higher energies due to optical loading. In addition to the X-ray fluorescence, there was evidence for an additional source of X-ray emission. This was indicated by (i) a faint X-ray halo around Mars which could be traced out to three Mars radii, and (ii) an additional component in the X-ray spectrum of Mars, which had a similar spectral shape as the halo.

In 1996, the discovery of comets as a new, unexpected class of bright X-ray sources [6; 7; 8] led to an increased interest in X-ray studies of solar system objects. It revealed the importance of another process for the generation of soft X-rays which seems to have been overlooked for a long time: charge exchange between highly charged heavy ions in the solar wind and neutral gas in the solar system [9]. With its tenuous atmosphere, the absence of a strong magnetic field, and orbiting at a heliocentric distance where comets ex-

hibit significant activity, Mars can be considered as a planetary analog to a comet. Thus, it was reasonable to expect that the same solar wind charge exchange processes which cause comets to emit X-rays would also operate at Mars.

The statistical significance of the Martian halo, however, was quite low, and all the information about it had to be derived from an excess of only  $34.6 \pm 8.4$  ( $1\sigma$ ) counts relative to the background. Within these very limited statistics, the general spectral properties of this component resembled those expected for charge exchange interactions between highly charged heavy ions in the solar wind and exospheric hydrogen and oxygen around Mars.

## 2. Mars observed with XMM-Newton

The situation improved considerably with the first observation of Mars with *XMM-Newton*, on November 19–21, 2003 [10; 11]. This observation confirms the presence of the Martian X-ray halo and makes for the first time a detailed analysis of its spectral, spatial, and temporal properties possible. It proves that the source of the X-ray emission is indeed charge exchange between highly charged solar wind ions and exospheric neutrals, providing the first definite detection of solar wind charge exchange (SWCX) induced X-ray emission from the exosphere of another planet. Furthermore, it unambiguously shows that the X-ray radiation which we observe from the planetary disk is primarily due to scattered solar X-rays.

Many of these results are based on high resolution imaging X-ray spectroscopy with *RGS*.

Table 1  
Emission lines in the *RGS* Mars spectra

line #	id	wavelength [Å]	energy [eV]	ion	line origin transition
1	Ne72	14.21	872.5	Ne <sup>7+</sup>	$2p \rightarrow 1s$
2	O74	15.18	817.0	O <sup>7+</sup>	$4p \rightarrow 1s$
3	O65	17.40	712.5	O <sup>6+</sup>	$5p \rightarrow 1s$
4	O72	18.97	653.6	O <sup>7+</sup>	$2p \rightarrow 1s$
5	N63	20.91	593.0	N <sup>6+</sup>	$3p \rightarrow 1s$
6	O6r	21.60	574.0	O <sup>6+</sup>	$2^1P_1 \rightarrow 1^1S_0$
7	O6i	21.81	568.5	O <sup>6+</sup>	$2^3P_1 \rightarrow 1^1S_0$
8	O6f	22.11	560.9	O <sup>6+</sup>	$2^3S_1 \rightarrow 1^1S_0$
9	CO2a	23.50	527.7	CO <sub>2</sub>	$1\pi_g \rightarrow 1s$
10	CO2b	23.68	523.5	CO <sub>2</sub>	$3\sigma_u \rightarrow 1s$
11	N62	24.78	500.3	N <sup>6+</sup>	$2p \rightarrow 1s$
12	C55	26.36	470.4	C <sup>5+</sup>	$5p \rightarrow 1s$
13	C54	26.99	459.4	C <sup>5+</sup>	$4p \rightarrow 1s$
14	C53	28.47	435.6	C <sup>5+</sup>	$3p \rightarrow 1s$
15	N22	31.51	393.5	N <sub>2</sub>	$2p \rightarrow 1s$
16	C45	32.75	378.5	C <sup>4+</sup>	$5p \rightarrow 1s$
17	C52	33.74	367.6	C <sup>5+</sup>	$2p \rightarrow 1s$

## 2.1. High resolution X-ray spectra of Mars

Although Mars is a very faint X-ray source, the sensitivity of *RGS* was sufficient for performing, for the first time ever, high resolution X-ray spectroscopy of the Martian atmosphere and exosphere [10]. *RGS* spectra taken at cross dispersion distances 15''..50'', corresponding to 2.5..8 Mars radii (Fig. 1a) reveal that there is extended X-ray halo around Mars, composed of many emission lines of similar flux. With the exception of lines #9 and #10, all these lines appear where emission is expected from the de-excitation of highly charged ions (Tab. 1). The lines #9 and #10 are caused by fluorescence of CO<sub>2</sub>. They appear in the halo spectrum only because of instrumental effects. However, these lines dominate in the *RGS* spectra from regions close to Mars (at cross dispersion distances of less than 10'' from its center; Fig. 1b), where also the N<sub>2</sub> fluorescence line (#15)

is indicated. These two high resolution spectra clearly show that the X-rays from Mars are composed of two completely different components.

In terms of spectral resolution, Fig. 1a shows perhaps the best charge exchange spectrum ever obtained. The high spectral resolution is demonstrated in Fig. 2a, which zooms to a small section covering only 3Å (70 eV). All the emission in this spectral region originates from inner shell electron transitions in oxygen, either six-fold ionized or neutral (embedded in CO<sub>2</sub>). This spectrum was compiled for cross dispersion distances  $\leq 50''$  and includes also emission from Mars itself. It is dominated by CO<sub>2</sub> fluorescent emission, which is clearly resolved into two lines (#9 and #10) of similar flux. This is probably the first astronomical measurement of fine structure in the X-ray fluorescence of CO<sub>2</sub>.

A straightforward explanation for the fact that we are observing two peaks instead of one is that in the CO<sub>2</sub> atmosphere of Mars, the oxygen atom is embedded in a molecule, where additional energy states are available for the electrons. The line at 528 eV (#9) is caused by an electron transition from the  $1\pi_g$  orbital (which is almost a pure  $2p$  orbital around the oxygen atom, and thus similar to the isolated oxygen atom state) into the ground state, while the line at 523 eV (#10) is a superposition of transitions from three orbitals,  $4\sigma_g$ ,  $3\sigma_u$ , and  $1\pi_u$ , into the ground state.

Even more exciting in Fig. 2a is the fine structure seen in the emission from O<sup>6+</sup> ions (lines #6, #7, #8). These lines are the result of electron transitions between the  $n = 2$  shell and the  $n = 1$  ground state shell. As O<sup>6+</sup> contains two electrons, there are two possible states of the ion, depending on the relative spin orientation of the electrons: singlet states (mainly  $^1S_0$  and  $^1P_1$ ) and triplet states (mainly  $^3S_1$  and  $^3P_{0,1,2}$ ). Because transitions from triplet states to the ground state require spin changes of the electrons, these are slow processes compared to transitions from singlet states.

The line #6 results from fast transitions from a singlet state ( $^1P_1$ ) with a decay rate of  $3.3 \cdot 10^{12} \text{ s}^{-1}$ , while the lines #7 and #8 are caused by slow transitions from triplet states. Particularly interesting is the line #8, because the corresponding transition starts from a metastable state ( $^3S_1$ ) and has a decay rate of only  $1.0 \cdot 10^3 \text{ s}^{-1}$ . This state can easily be depopulated by colli-

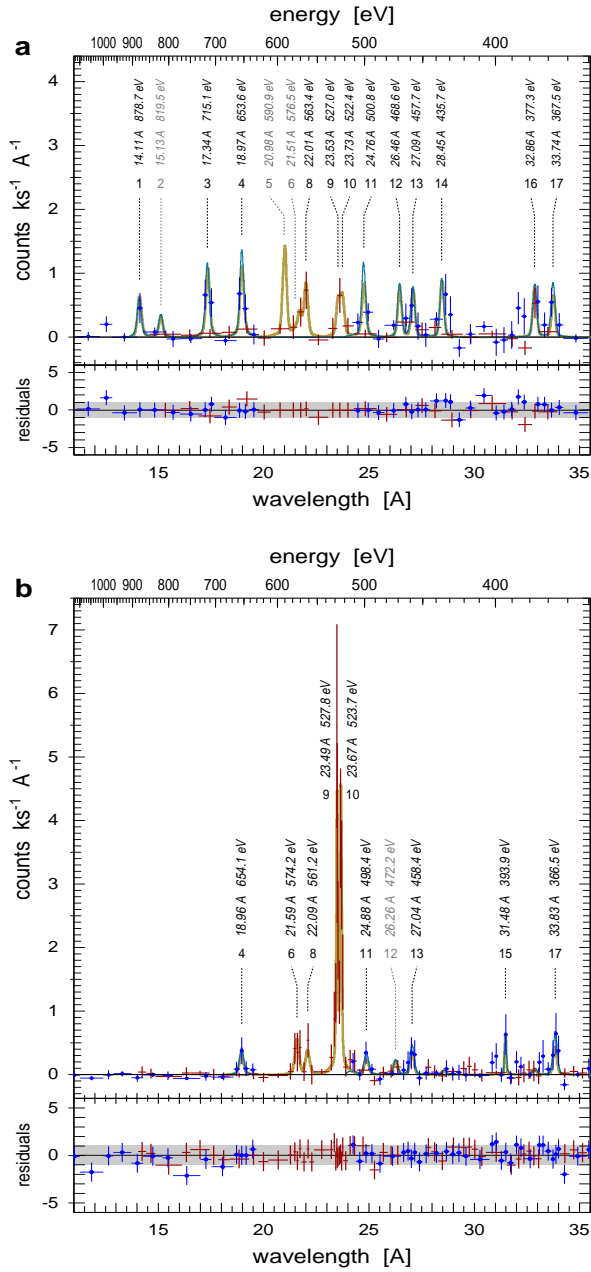


Figure 1. *XMM-Newton/RGS* spectra of Mars and its halo, accumulated at cross dispersion distances **a)** 15''.. 50'' and **b)** 0''..10'' from the center of Mars. Smooth curves show the corresponding folded model spectra, with a thick line for *RGS1* and a thin one for *RGS2*. The positions resulting from the fit are written above each line, together with a running number, for easier reference (cf. Tab. 1). A zoomed version of the central region around 23 Å / 540 eV is shown in Fig. 2a.

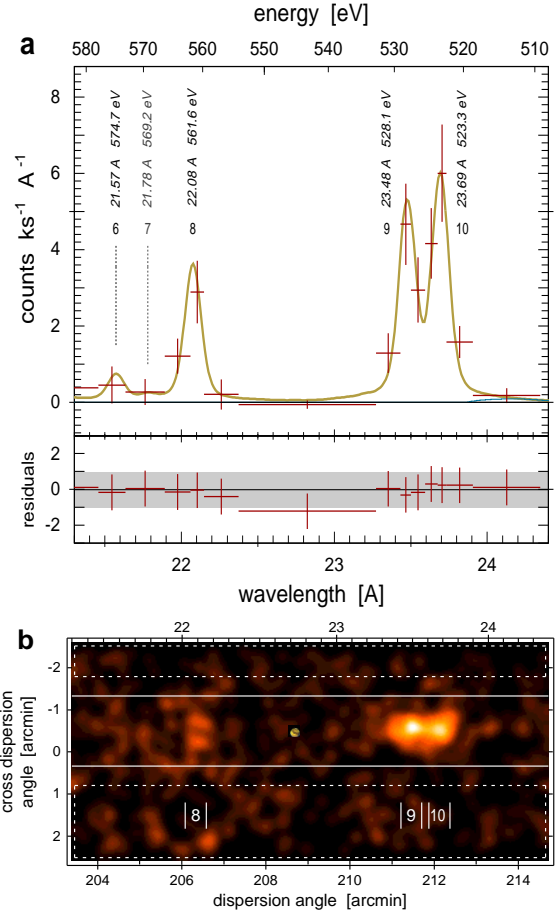


Figure 2. **a)** *XMM-Newton/RGS1* spectrum of Mars and its halo at cross dispersion distances 0''.. 50'' from the center of Mars, showing the region around the  $\text{CO}_2$  doublet and the  $\text{O}^{6+}$  multiplet. **b)** Dispersed image in the same wavelength/energy scale as in (a). This image was binned into  $2'' \times 2''$  pixels and smoothed with a Gaussian function with  $\sigma = 8'' \times 8''$ . It contains the full FOV of *RGS* along the cross dispersion direction. The inner rectangle shows the extraction region for the spectrum in (a); the background was taken from the two dashed bands above and below. An optical image (taken by the author with a 4'' Newton telescope) is inserted at the center to illustrate the angular size of Mars during the observation; the observed X-ray images are blurred mainly by the PSF of the telescope. Note that due to the high dispersion of *RGS*, the X-ray image of the Martian halo (8) is completely detached from the fluorescent images (9, 10).

sions before the transition takes place. The fact that the line #8 is considerably brighter than the lines #6 and #7 excludes thermal or collisional excitation as the origin of the Martian X-ray halo emission. For hot plasmas, the flux ratio  $G = (\#7 + \#8) / \#6$  of triplet to singlet transitions is usually less than one [e.g. 12].

However, if the emission lines result from electron capture by multi-charged ions colliding with neutral gas at low density, the situation is completely different. In this case,  $G$  is predicted to be in excess of three [13]. The value of the  $G$  ratio for the  $O^{6+}$  emission induced by the interaction between the solar wind ions and heliospheric hydrogen gas has been evaluated as 6.7 [14], and for the cometary X-rays as 5.8 [15]. These values agree well with that derived from the Mars *RGS* spectra:  $G \sim 6$  within 8 Mars radii. Thus, the high resolution X-ray spectrum in Fig. 2a provides the direct proof that the X-ray emission of the Martian halo is indeed caused by the SWCX process.

## 2.2. X-ray images of Mars in individual emission lines

As slitless spectrometers, the *RGS* produce in each spectral line an image of the observed object. Due to the high dispersion of the *RGS* and the small spatial extent of Mars, there is essentially no overlap between the individual images. This makes it possible to study the spatial structure of the X-ray emission in individual spectral lines. As fluorescence occurs in neutral atoms and molecules, while charge exchange involves highly charged ions, the energies/wavelengths of the corresponding emission lines are different. Thus, the contributions of fluorescence and charge exchange can be completely separated by this method.

Figure 2b shows the *RGS* image which corresponds to the zoomed spectrum in Fig. 2a, at the same wavelength scale. To illustrate the spatial extent of Mars at the time of the observation, an optical image was inserted at the center. The spectral images of the  $CO_2$  emission to the right (#9, #10) prove that this radiation originates close to the planet, as their brightness distributions peak at the position of Mars. Brightness profiles along the cross dispersion direction show that their extent is consistent with the size of Mars, if the instrumental blur is taken into account, and that there is no significant difference

between both components.

The spectral image of the  $O^{6+}$ :  $^3S_1 \rightarrow ^1S_0$  transition (#8) is completely different from that of the  $CO_2$  emission, exhibiting two distinct blobs along the cross dispersion direction (which is approximately the North–South direction on Mars), with practically no emission in between. This means that the emission does not originate close to Mars or in an X-ray luminous extended shell around it, but at two well localized regions  $\sim 3000$  km above both poles. For other emission lines, however, the morphology is different. Figure 3 presents spectral images for the major emission lines, identified by the abbreviations listed in Tab. 1. These images reveal differences in the spatial structures, not only between fluorescence and charge exchange, but also between different ions and ionization states.

The structure seen in the spectral image of O6f seems to be a specific property of emission from ionized oxygen, as the O72 image (Fig. 3a) also shows two distinct blobs along the cross dispersion direction. Compared to O6f (Fig. 3b), the O72 emission occurs at larger distances from Mars. There is also some evidence in Fig. 3a that the peak of the O72 emission is shifted to the right with respect to Mars. Interpreted as redshift, this would indicate velocities of  $O^{8+}$  ions in excess of  $\sim 400$  km s $^{-1}$  along the line of sight, as the dashed vertical lines in Fig. 3a indicate. Alternatively, this shift may be interpreted as a spatial displacement.

Spectral images can also be obtained for the carbon emission lines C53 and C52 (Fig. 3d,e). These images show yet another morphology: there is again clear evidence for extended, unisotropic emission, but unlike the blobby O72 and O6f appearance, the C53 and C52 emissions exhibit a more band-like structure without a pronounced intensity dip at the position of Mars. There is also evidence that at larger distances from Mars the emission is shifted towards the right. For comparison, the morphology of the fluorescent radiation (Fig. 3g-i), is clearly concentrated to the planet. While an interpretation of the fluorescence images is straightforward, an interpretation of the structures in the halo emission is not an easy task, since they depend on many parameters [e.g. 16].

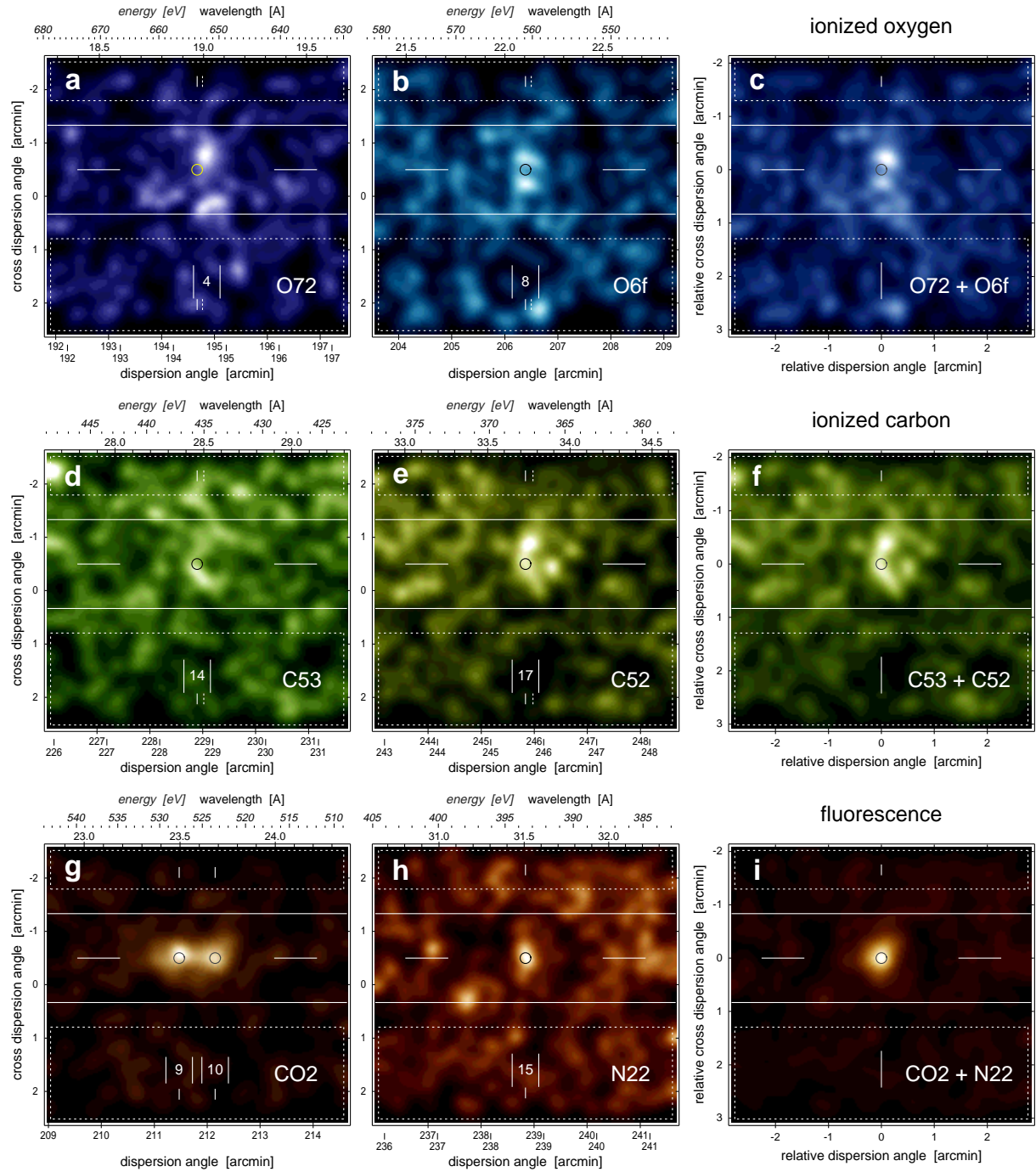


Figure 3. *XMM-Newton/RGS* images of Mars and its halo in the individual emission lines of ionized oxygen (top row), ionized carbon (middle row), and fluorescence of CO<sub>2</sub> and N<sub>2</sub> molecules (bottom row). The images were corrected for exposure variations, were binned into  $2'' \times 2''$  pixels and smoothed with a Gaussian function with  $\sigma = 8'' \times 8''$ . All are displayed at the same angular scale; the dynamic scale, however, was individually adjusted. The images in the rightmost column are the sum of the images to their left. For the wavelengths/energies of the emission lines, the values in Tab. 1 were used. These are indicated by the short vertical lines and the circle in the middle, which illustrates the size and expected position of Mars at these emission lines. Dashed vertical lines in the frames a,b,d,e indicate the apparent shift along the dispersion direction for a redshift of  $400 \text{ km s}^{-1}$ . The projected direction to the Sun is towards the left.

### 3. Summary and conclusions

X-rays from Mars consist of two different components: (i) solar X-rays scattered in the upper Martian atmosphere, and (ii) emission from highly charged heavy solar wind ions in excited states, resulting from charge exchange interactions with neutrals in the Martian exosphere. For both components, the pioneering observations with *Chandra* and *XMM-Newton* have shown how X-ray observations will provide novel methods for studying this planet: high resolution X-ray images of Mars in the fluorescence lines of C,N,O will make it possible to investigate the atmospheric layers above  $\sim 80$  km, which are difficult to study otherwise, and their response to solar activity, while X-ray images of Mars in the lines of excited ions will enhance our knowledge about the Martian exosphere and its interaction with the solar wind.

It is remarkable that *XMM-Newton* has the capability to trace the exospheric X-ray emission, with high spectral resolution, out to  $\sim 8$  Mars radii ( $\sim 27\,000$  km), proceeding into exospheric regions far beyond those that have been observationally explored to date. This is particularly interesting because the X-ray emission results directly from charge exchange interactions between atmospheric constituents and solar wind ions, a process which is considered as an important non-thermal escape mechanism and which may be responsible for a significant loss of the Martian atmosphere. Despite this importance, our observational knowledge of the Martian exosphere is still poor. Thus, X-ray observations, providing a novel method for studying exospheric processes on a global scale, may lead to a better understanding of the present state of the Martian atmosphere and its evolution. They open up a completely new possibility of remote, global, imaging of planetary exospheres, and their spatial and temporal variability.

In addition to its importance to planetary studies, the possibility to obtain from X-ray observations of Mars not only charge exchange spectra with unprecedented spectral resolution, but also images of the morphological structures originating from specific electron transitions in individual ions, is likely to contribute to an improved understanding of the physics of charge exchange, which is of general importance to X-ray plasma diagnostics, both in the laboratory and in outer space.

### References

- [1] Winckler, J. R., Peterson, L., Arnoldy, R., & Hoffman, R. 1958, *Phys. Rev.*, 110, 1221
- [2] Grader, R. J., Hill, R. W., & Seward, F. D. 1968, *J. Geophys. Res.*, 73, 7149
- [3] Metzger, A. E., Gilman, D. A., Luthey, J. L., et al. 1983, *J. Geophys. Res.*, 88, 7731
- [4] Dennerl, K., Burwitz, V., Englhauser, J., Lisse, C., & Wolk, S. 2002, *A&A*, 386, 319
- [5] Dennerl, K. 2002, *A&A*, 394, 1119
- [6] Lisse, C. M., Dennerl, K., Englhauser, J., et al. 1996, *Science*, 274, 205
- [7] Dennerl, K., Englhauser, J., & Trümper, J. 1997, *Science*, 277, 1625
- [8] Mumma, M. J., Krasnopolsky, V. A., & Abbott, M. J. 1997, *ApJ*, 491, L125
- [9] Cravens, T. E. 1997, *Geoph. Res. Lett.*, 24, 105
- [10] Dennerl, K., Lisse, C. M., Bhardwaj, A., et al. 2006, *A&A*, accepted for publication
- [11] Dennerl, K., Lisse, C. M., Bhardwaj, A., et al. 2006, *A&A*, in preparation
- [12] Smith, R. K., Brickhouse, N. S., Liedahl, D. A., & Raymond, J. C. 2001, *ApJ*, 556, L91
- [13] Kharchenko, V., Rigazio, M., Dalgarno, A., & Krasnopolsky, V. A. 2003, *ApJ*, 585, L73
- [14] Pepino, R., Kharchenko, V., Dalgarno, A., & Lallement, R. 2004, *ApJ*, 617, 1347
- [15] Kharchenko, V. 2005, in *X-ray diagnostics of Astrophysical Plasmas: Theory, Experiment, and Observation*, ed. R. K. Smith, Vol. 774, 271
- [16] Gunell, H., Holmström, M., Kallio, E., Janhunen, P., & Dennerl, K. 2005, *Adv. Space Res.*, 36, 2057

### ACKNOWLEDGEMENTS

This work is based on observations obtained with *XMM-Newton*, an ESA science mission with instruments and contributions directly funded by ESA Member States and NASA. In Germany, the *XMM-Newton* project is supported by the Bundesministerium für Bildung und Forschung/Deutsches Zentrum für Luft- und Raumfahrt (BMBF/DLR), the Max-Planck-Gesellschaft, and the Heidenhain-Stiftung.